

Gaseous viscous peeling of linearly elastic substrates

Shai B. Elbaz, Hila Jacob and Amir D. Gat

Faculty of Mechanical Engineering, Technion - Israel Institute of Technology, Haifa 3200003, Israel

(Received 2017)

We study pressure-driven propagation of gas into a micron-scale gap between two linearly elastic substrates. Applying the lubrication approximation, the flow-field is governed by the interaction between elasticity and viscosity, as well as weak rarefaction and low-Mach-compressibility, characteristic to gaseous microflows. Several physical limits allow simplification of the governing evolution equation and enable solution by self-similarity. These limits correspond to different time-scales and physical regimes which include compressibility-elasticity-viscosity, compressibility-viscosity and elasticity-viscosity dominant balances. For a prewetting layer thickness which is similar to the elastic deformation generated by the background pressure, a symmetry between compressibility and elasticity allows to obtain a self-similar solution which includes weak rarefaction effects. The results are validated by numerical solutions of the evolution equation.

1. Introduction

In this work we analyze the propagation of a Newtonian ideal gas into a thin gas-filled gap, with thickness of the order of microns, bounded by linearly elastic substrates. At standard atmospheric conditions, pressure-driven gaseous flows within micron-sized configurations involve significant viscous resistance, yielding 'low-Mach-compressibility' with negligible inertial effects (Taylor & Saffman 1957; Arkilic *et al.* 1997). In addition, weak rarefaction effects emanating from Knudsen numbers at the range of $Kn \approx 0.01$ to ≈ 0.1 yield velocity- and temperature-slip at the solid boundaries (Cercignani 2000). Thus, gaseous viscous peeling is governed by interaction of elasticity of the boundaries, gas viscosity, low-Mach-compressibility and weak-rarefaction.

The limit of large deformations compared with the initial gap corresponds to viscous peeling dynamics which are characterized by a distinct peeling front, similarly to the fronts in free-surface flows (Oron *et al.* 1997) and gravity currents (e.g. Huppert 1982). McEwan & Taylor (1966) were the first to examine viscous peeling, and studied the removal of an adhesive strip from a rigid surface. While previous studies modelled the adhesive as a Hookean elastic material, McEwan & Taylor (1966) examined the opposite limit of a Newtonian viscous fluid, which enabled calculation of the peeling speed as a function of the applied tension. Other works involving viscous peeling dynamics include Hosoi & Mahadevan (2004), who examined the peeling and levitation of a elastic sheet over a thin viscous film and Lister *et al.* (2013) who studied axisymmetric viscous peeling of an elastic sheet from a flat rigid surface by injection of fluid between the surface and the sheet (additional relevant works include Hodges & Jensen 2002; Hewitt *et al.* 2015; Thorey & Michaut 2016; Elbaz & Gat 2016; Young & Stone 2017).

Effects of weak rarefaction and 'low-Mach-compressibility' on pressure driven flows were extensively studied in the context of gaseous micro-fluidics (Gad-El-Hak 1999; Ho & Tai 1998). The first experimental works were conducted by Pong *et al.* (1994) and

Liu *et al.* (1995) and presented non-constant pressure gradient in uniform micro-channels associated with 'low-Mach-compressibility' effects. Arkilic *et al.* (1997) and Zohar *et al.* (2002) analytically and experimentally studied gas flow through a uniform long micro-channel with both compressibility and velocity-slip effects (among others such as Aubert & Colin 2001; Jang & Wereley 2004). Gaseous flows through shallow non-uniform micro-channels involving bends, constrictions and cavities were studied experimentally by Yu *et al.* (2005); Lee *et al.* (2001, 2002) and treated analytically by Gat *et al.* (2008, 2009, 2010*b,a*).

The aim of the current work is to study gaseous viscous peeling dynamics involving low-Mach-compressibility and weak-rarefaction. The structure of this work is as follows: In §2 we define the problem and develop the evolution equation. In §3.1 we present an implicit steady-state solution. In §3.2 we present self-similar solutions of the evolution equation for various limits and map the transitions between the different regimes. In §3.3 we develop a self-similar solution which includes weak-rarefaction effects for configurations which involve symmetry between elasticity and compressibility. Concluding remarks are presented in §4.

2. Problem formulation and derivation of the evolution equation

We examine pressure-driven gaseous viscous peeling of a two dimensional gap bounded by linear elastic substrates. The configuration (similar to Gaver *et al.* (1996)) is illustrated in figure 1. The $x - y$ coordinate system is located at the center of the gap at rest, where x is parallel to the gap streamwise direction, time is t , and temperature is θ . At rest, the constant gap between the lower and upper substrates is denoted by h_0 , and contains gas at the background pressure p_a . Film height is denoted by $h = h_0 + d$, where $d = d_u + d_l$ is the combined pressure induced vertical deformation of the upper and lower surfaces. The stiffness coefficients of the upper and lower distributed spring substrates are k_u and k_l , respectively, where we define total channel stiffness by $k = (k_u^{-1} + k_l^{-1})^{-1}$. Gas velocity is (u, v) , absolute pressure is p , gas viscosity is μ , gas density is ρ , the gas constant is r_g and the gas mean-free-path is λ .

We define l as the axial length-scale of the configuration and p^* as characteristic gauge pressure (representing the characteristic value of $p - p_a$). Thus the characteristic elastic displacement is given by p^*/k . We define the dimensionless ratios

$$Kn = \frac{\lambda}{h_0 + d} = Kn_a \left(\frac{p_a}{p} \right) \left(\frac{h_0}{h_0 + d} \right), \quad \Pi_H = \frac{h_0 k}{p^*}, \quad \Pi_P = \frac{p_a}{p^*}, \quad (2.1)$$

where Kn is the Knudsen number representing the validity of the continuum assumption; Kn_a corresponds to the Knudsen number at the background pressure and the initial gap h_0 ; Π_H is the ratio of initial gap to the elastic displacements and Π_P is the ratio of the external background pressure to p^* . The limit $\Pi_P \rightarrow \infty$ corresponds to negligible low-Mach-compressibility and the limit $\Pi_H \rightarrow \infty$ corresponds to negligible elastic deformations.

Hereafter we denote normalized variables by Capital letters. Scaling according to the lubrication approximation, the corresponding normalized parameters and variables are the coordinates $(X, Y) = (x/l, yk/p^*)$, time $T = t(p^*)^2/k^2 l^2 \mu$, total elastic vertical displacement $D = dk/p^*$, film height $H = hk/p^* = \Pi_H + D$, fluid velocity $(U, V) = (uk^2 \mu l / (p^*)^3, vk^3 \mu l^2 / (p^*)^4)$, pressure $P = p/p^*$ and density $\Lambda = \rho / (p^*/r_g \theta)$.

We assume isothermal flow and negligible body forces, which is common practice for flows through micron-sized configurations (e.g. Arkilic *et al.* 2001; Zohar *et al.* 2002). Applying the above scaling, the requirements for the validity of the lubrication approxi-

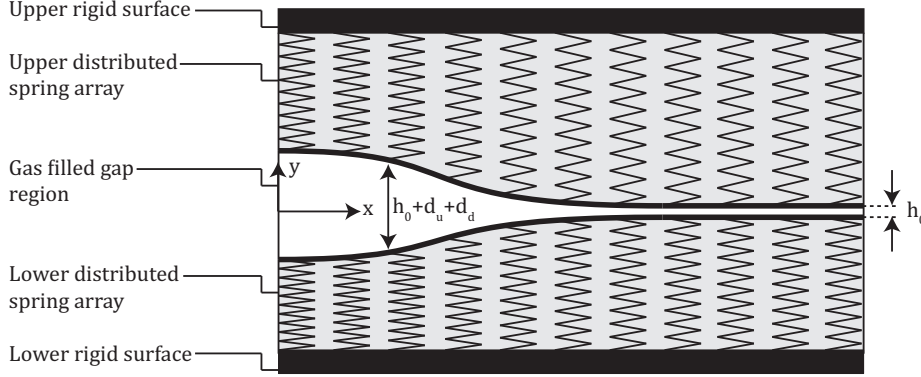


Figure 1: A schematic description of the configuration: A gas-filled gap separates two parallel distributed linear spring arrays bounded by rigid surfaces. The initial prewetting gas layer is denoted by h_0 and upper and lower vertical deformations are denoted by d_u and d_d , respectively.

mation are given by the following relations,

$$\varepsilon = \frac{p^*}{kl} \ll 1, \quad \alpha^2 = \varepsilon Re = \frac{(p^*)^6}{r_g \theta k^4 \mu^2 l^2} \ll 1 \quad (2.2)$$

where ε represents the slenderness of the configuration, α^2 is the Womersley number and εRe is the reduced Reynolds number. Applying (2.2) allows to utilize the standard lubrication form of the momentum equations, $\partial P / \partial X \sim \partial^2 U / \partial Y^2$, $\partial P / \partial Y \sim 0$, compressible conservation of mass equation, $\partial \Lambda / \partial T + \partial (\Lambda U) / \partial X + \partial (\Lambda V) / \partial Y = 0$ and isothermal equation of state $\Lambda = P$.

The validity of the continuum assumption requires a sufficiently small Knudsen number $Kn = \lambda / h_0$, defined here as the ratio between the molecular mean-free-path λ and the prewetting layer thickness h_0 . While for $Kn < 10^{-3}$ use of the no-slip boundary condition is appropriate, for gas flows through micron-sized configurations at standard atmospheric conditions $Kn \approx 10^{-1} - 10^{-2}$. This Knudsen regime requires the incorporation of velocity-slip, and thus the boundary conditions are given by the Navier-slip condition,

$$[U(Y = D_u), U(Y = D_l)] = \sigma \frac{Kn_a \Pi_H \Pi_P}{P} \left[-\frac{\partial U(Y = D_u)}{\partial Y}, \frac{\partial U(Y = D_l)}{\partial Y} \right] \quad (2.3a)$$

as well as the kinematic boundary condition at the gas-substrate interface

$$[V(Y = D_u), V(Y = D_l)] = \frac{1}{2} \left[\frac{\partial D_u}{\partial T} + U(Y = D_u) \frac{\partial D_u}{\partial X}, \frac{\partial D_l}{\partial T} + U(Y = D_l) \frac{\partial D_l}{\partial X} \right], \quad (2.3b)$$

where the coefficient σ represents the interaction between the gas molecules and the solid wall (Chapman & Cowling 1952).

Applying (2.3a) to the X -momentum equation yields the velocity profile,

$$U = \frac{1}{2} \frac{\partial P}{\partial X} \left(Y^2 - \frac{(D + \Pi_H)^2}{4} - \frac{\sigma Kn_a \Pi_H \Pi_P}{2} \frac{(D + \Pi_H)}{P} \right). \quad (2.4)$$

Integration of mass conservation equation in conjunction with (2.3b)- (2.4), and applying

the normalized linear elastic relation $D = P - \Pi_P$, yields the evolution equation

$$\frac{\partial}{\partial \mathfrak{T}} [(D + \Pi_H)(D + \Pi_P)] = \frac{\partial}{\partial X} \left[\left((D + \Pi_P)(D + \Pi_H)^3 + 6\sigma K n_a \Pi_H \Pi_P (D + \Pi_H)^2 \right) \frac{\partial D}{\partial X} \right], \quad (2.5)$$

where hereafter $\mathfrak{T} = T/12$ for convenience.

3. Solutions of the evolution equation

3.1. Steady-state

An implicit solution of (2.5) may be obtained for steady-state flow in a finite configuration with prescribed pressures at the inlet and outlet sections ($D(0) = P(0) - \Pi_P$ and $D(1) = P(1) - \Pi_P$, respectively),

$$X(D) = \frac{F(D) - F(D(0))}{F(D(1)) - F(D(0))}, \quad (3.1a)$$

where

$$F(D) = 40\sigma K n_a \Pi_H \Pi_P (D + \Pi_H)^3 + 5(D - \Pi_P)(D + \Pi_H)^4 - (D + \Pi_H)^5. \quad (3.1b)$$

Solution (3.1) is depicted in figure 2(a) for the case of $\Pi_P = 1$, $P(0)/P(1) = 2$, $K n_a = 0$ (smooth lines) and $K n_a = 0.1$ (dashed lines) for various values of Π_H . Small values of Π_H represent large ratios of elastic deformation to initial gap h_0 , which reduce the pressure gradient near the inlet while increasing it towards the outlet. For constant prewetting layer thickness and background pressure (i.e. constant $K n_a$), decreasing Π_H decreases the local Knudsen number (as seen in panel (b)) and thus decrease the effect of weak rarefaction on the pressure distribution. Panel (c) presents the effect of weak rarefaction on the mass-flow-rate vs. Π_H . Weak rarefaction effects on mass-flow-rate tend to a constant finite value for $\Pi_H \rightarrow \infty$, and decreases with Π_H . Panel (d) presents the mass-flow-rate vs. the pressure difference for various values of Π_H . While the gradient of the different lines vary significantly with Π_H for the limit of small pressures at the inlet, as the inlet pressure increases the viscous resistance no longer depends on Π_H (or h_0) and the gradients converge.

3.2. Self-similar Barenblatt solutions for negligible rarefaction effects

While exact solutions of (2.5) are not available, several limits involving negligible rarefaction effects yield known self-similar solutions. Furthermore, the flow-field may be described by different approximate solutions during different time-scales of observation of the peeling process. Physical insight may thus be gained by mapping the different approximate solutions and the corresponding time-scales and transitions.

We focus on fundamental solutions for the case of impulse driven peeling - an abrupt release of a finite mass at $T = 0$ into the inlet at $X = 0$. This process is characterized by a compactly supported region of displacement and a distinct front, denoted by X_F . The relevant integral form of mass conservation is

$$\int_0^{X_F} [(D + \Pi_H)(D + \Pi_P) - \Pi_H \Pi_P] dX = M, \quad (3.2)$$

where M is a constant representing the mass injected into the interface at $T = 0$. The conditions near the contact line $X \rightarrow X_F$ are $D \rightarrow 0$ and $P \rightarrow \Pi_P$.

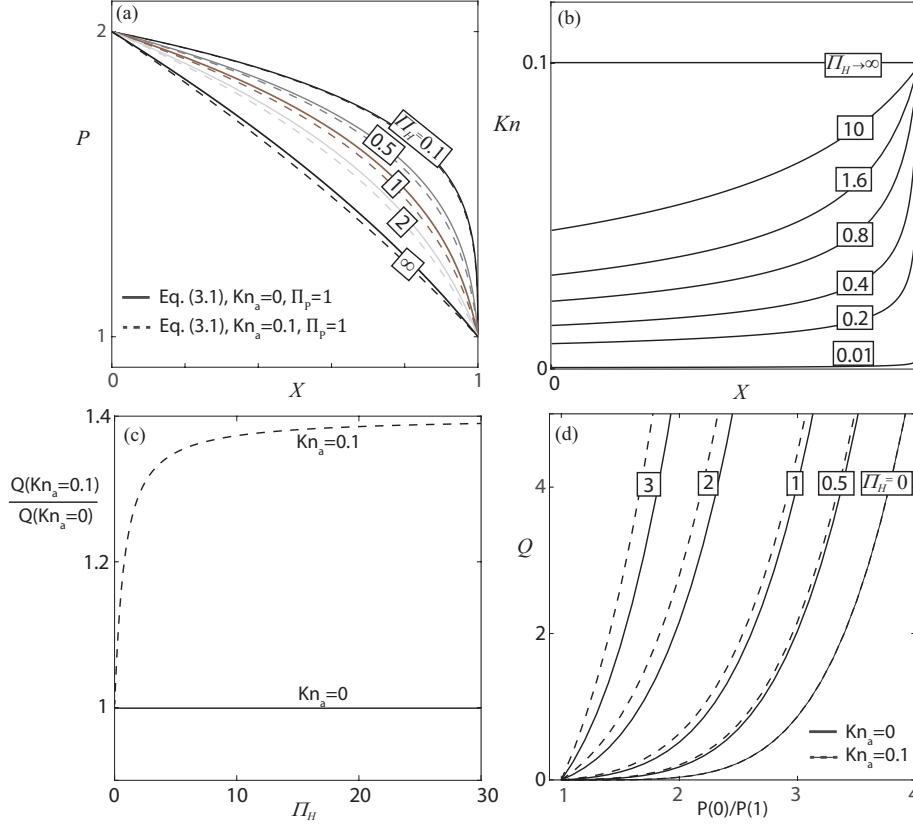


Figure 2: Steady-state solution (3.1) of gaseous viscous flow in a 2D gap bounded by linearly elastic substrates. Gas pressure (a) and local Knudsen (b) profiles vs. X for varying Π_H for $P(0)/P(1) = 2$. (c) Mass flow rate vs. Π_H for $Kn_a = 0$ and $Kn_a = 0.1$. (d) Mass flow rate vs. pressure ratio $P(X=0)/P(X=1)$ for various values of Π_H . For all panels $Kn_a = 0.1$, $\sigma = 1$ and $\Pi_P = 1$.

Due to the sudden injection of mass at the inlet, for all values of Π_P, Π_H , we obtain that for sufficiently early times $D \gg \Pi_P, \Pi_H$, yielding an early regime in which both elasticity and compressibility contribute to the peeling process. However, for injection of mass at small but finite time-scales there is an initial value of the characteristic gauge pressure (denoted hereafter by p_0^*), scaling by which yields $D \sim O(1)$ for early times. This sets the requirement $\Pi_P, \Pi_H \ll 1$ as a condition for the appearance of the early time regime (i.e. large gauge pressure compared with background pressure and large displacement to prewetting thickness ratio). In this early time regime the leading order of equation (2.5) is a porous-medium-equation of order 2.5 for the variable D^2 . Applying ZKB's solution (Barenblatt 1952) yields the time propagation rate $X_F = O(\mathfrak{T}^{2/7})$ and the peeling dynamics are given by,

$$D(X, \mathfrak{T}) = \left(\frac{1}{5}\right)^{-1/7} \mathfrak{T}^{-1/7} \left[C_1 - \frac{3}{35} \left(\frac{1}{5}\right)^{-4/7} X^2 \mathfrak{T}^{-4/7} \right]_+^{1/3}, \quad (3.3a)$$

$$C_1 = \left(\frac{2M}{S_1}\right)^{6/7}, \quad S_1 = \sqrt{\frac{35\pi}{3} \frac{B(1/2, 5/3)}{\Gamma(1/2)}}, \quad (3.3b)$$

where B is the beta function, Γ the gamma function and $(s)_+ = \max(s, 0)$. As the added mass propagates and expands into the substrate, the gas pressure decreases and thus D decreases, eventually invalidating the requirement of $D \gg \Pi_P, \Pi_H$. This sets a validity time range of $\mathfrak{T} \ll 5C_1^{7/3}/\max(\Pi_P^7, \Pi_H^7)$ for (3.3) based on $D(X=0)$.

For the case of $\Pi_H/\Pi_P = h_0/(p_a/k) \gg 1$ (corresponding to negligible effects of elasticity and dominant effects of low-Mach-number gas compressibility) an intermediate regime exists where $\Pi_P \ll D \ll \Pi_H$. In this regime, the leading order of equation (2.5) is a porous-medium-equation of order 2 for D . Thus the solution will transition to a propagation rate of $X_F = O(\mathfrak{T}^{1/3})$ and the resulting profile,

$$D(X, \mathfrak{T}) = \left(\frac{\Pi_H^2}{2}\right)^{-1/3} \mathfrak{T}^{-1/3} \left[C_2 - \frac{1}{12} \left(\frac{\Pi_H^2}{2}\right)^{-2/3} X^2 \mathfrak{T}^{-2/3} \right]_+, \quad (3.4a)$$

$$C_2 = \left(\frac{2M}{\Pi_H S_2}\right)^{2/3}, \quad S_2 = \sqrt{12\pi} \frac{B(1/2, 2)}{\Gamma(1/2)}, \quad (3.4b)$$

will emerge in intermediate times with a validity range of $2C_2^3/\Pi_H^5 \ll \mathfrak{T} \ll 2C_2^3/\Pi_H^3 \Pi_P^2$. Solution (3.4) represents the limit of dominant gas compressibility, and is identical to the evolution of compressible low-Reynolds-number gas flow in rigid configurations. The relevant time-scale of this limit is $t^* = \mu/p^* \varepsilon^2$.

Alternatively, for $\Pi_P/\Pi_H = p_a/kh_0 \gg 1$, a different intermediate region exists for which $\Pi_H \ll D \ll \Pi_P$ and the leading order evolution equation is a porous-medium-equation of order 4 for D , yielding

$$D(X, \mathfrak{T}) = \left(\frac{1}{4}\right)^{-1/5} \mathfrak{T}^{-1/5} \left[C_3 - \frac{3}{40} \left(\frac{1}{4}\right)^{-2/5} X^2 \mathfrak{T}^{-2/5} \right]_+^{1/3}, \quad (3.5a)$$

$$C_3 = \left(\frac{2M}{\Pi_P S_3}\right)^{6/5}, \quad S_3 = \sqrt{\frac{40\pi}{3}} \frac{B(1/2, 4/3)}{\Gamma(1/2)}, \quad (3.5b)$$

with an $X_F = O(\mathfrak{T}^{1/5})$ spread-rate, typical of the early time propagation of the incompressible peeling problem (e.g. Elbaz & Gat 2016), and a validity range of $4C_3^{5/3}/\Pi_P^5 \ll \mathfrak{T} \ll 4C_3^{5/3}/\Pi_H^5$.

By setting larger values for Π_H or Π_P , propagation dynamics may skip or move across a certain stage in the sequence. All solutions will ultimately settle on $X_F = O(\mathfrak{T}^{1/2})$ propagation as $\mathfrak{T} \rightarrow \infty$ whether be it the prewetting thickness ratio Π_H or background to gauge pressure ratio Π_P the final regularization mechanism which linearizes (2.5).

The evolution of the solution through the various regimes and corresponding propagation rates is validated numerically in figure 3(a). A flow-chart illustrating the transitions and presenting the requirements for the different limits, as well as the time-ranges in which the limits are valid, is presented in figure 3(b). The validity range for each limit is calculated by requiring the appropriate order of magnitude of D for the examined limit from the solutions (3.3), (3.4) and (3.5) at $X=0$. The conditions (1) – (6) presented in figure 3(b) may be represented in dimensionless form as (1) $\Pi_P \gg 1$ and $\Pi_H \ll 1$; (2) $\Pi_P \ll 1$ and $\Pi_H \ll 1$; (3) $\Pi_P \ll 1$ and $\Pi_H \gg 1$; (4) $\Pi_H \ll \Pi_P$; (5) $\Pi_H \sim \Pi_P$; and (6) $\Pi_H \gg \Pi_P$. An additional solution with velocity-slip (dashed line) was also considered along with its no-slip counterpart marked by (2) + (5). For intermediate times Knudsen-diffusion is shown to mildly alter the spread rate, but this effect is reduced at the early time limit (3.3) as well as in the linearized regime. Figure 3(a) is supplemented by figure 4 which presents the numerical deformation profiles for various limits and the

convergence of the numerical profile to the theoretical results presented in (3.3), (3.4) and (3.5), corresponding to panels (a), (b) and (c), respectively.

3.3. Self-similar solution with weak rarefaction effects for $\Pi_P \rightarrow \Pi_H$

For the limit of $\Pi_H \rightarrow \Pi_P$ (or $k \rightarrow p_a/h_0$), applying $f = D + \Pi_H = D + \Pi_P$ allows to obtain an additional self-similar solution for the case of suddenly applied fixed inlet pressure. In this limit both the viscous and Knudsen diffusion terms of equation (2.5) will enforce a $O(\mathfrak{T}^{1/2})$ spread-rate and an exact self-similar solution with velocity-slip may be attained for $f(\eta)$, where $\eta = X\mathfrak{T}^{-1/2}$.

Substitution of $f(\eta)$ into (2.5) yields the self-similar boundary value problem,

$$f^{5''} + 10\sigma Kn_a \Pi_H^2 f^{3''} + \frac{5\eta}{2} f^{2'} = 0, \quad (3.6a)$$

supplemented by

$$f(0) = 1 + \Pi_H, \quad f(\infty) = \Pi_H, \quad (3.6b)$$

and

$$\int_0^\infty H^2(X, \mathfrak{T}) dX = M\mathfrak{T}^{1/2}, \quad M = \int_0^\infty f^2(\eta) d\eta. \quad (3.6c)$$

Self-similar profiles for various values of Π_H are presented in figure 5(a) for $Kn_a = 0$ (smooth lines) and $\sigma = 1$, $Kn_a = 0.1$ (dashed lines). The effect of weak rarefaction is shown to increase the speed of gas propagation, and reduce the gradients of the deformation. This effect decreases as Π_H and Π_P decrease, since Kn_a is defined ahead of the front, while the local Knudsen decreases as the gap and pressure increase (see (2.1)). For small Π_P and Π_H , the pressure and gap in the peeled region are greater compared with the background pressure p_a and prewetting layer thickness h_0 . This yields a significantly smaller effective Knudsen number in the peeled region, as illustrated in figure 5(b).

4. Concluding remarks

The propagation of a gas into micron-sized configurations with linearly elastic boundaries is governed by interaction between effects of low-Mach-compressibility, weak rarefaction, elasticity and viscosity. While exact solutions of the governing nonlinear evolution equation are not available, several limiting cases allow solution by self-similarity. These limits correspond to different physical regimes, including: (i) dominant balance between compressibility and viscosity, (PME of order 2) characterizing compressible flow in rigid micro-channels, (ii) dominant balance between elasticity and viscosity, (PME of order 4) characterizing incompressible flow in elastic micro-channels, and (iii) dominant balance involving viscosity, elasticity and compressibility (PME of order 2.5). During gas film propagation, the flow-field transitions between the aforementioned regimes and corresponding exact solutions. A map of these transitions was presented as a function of the prewetting layer thickness, the background pressure and stiffness of the spring array. The case where $kh_0 \approx p_a$ represents symmetry between compressibility and elasticity, and allowed to obtain an additional self-similar solution accounting for weak rarefaction effects.

While the steady-state solution presented in §3.1 is implicit, explicit solutions may be obtained for the same physical limits examined in the transient dynamics, as presented in §3.2. For negligible slip $Kn_0 \rightarrow 0$, steady-state solutions corresponding to the Barrenblatt self-similar limits (3.3)-(3.5) can be presented by the relation

$$D(X) = [(D(1) + C)^N - (D(0) + C)^N] X + (D(0) + C)^N]^{\frac{1}{N}} - C, \quad (4.1)$$

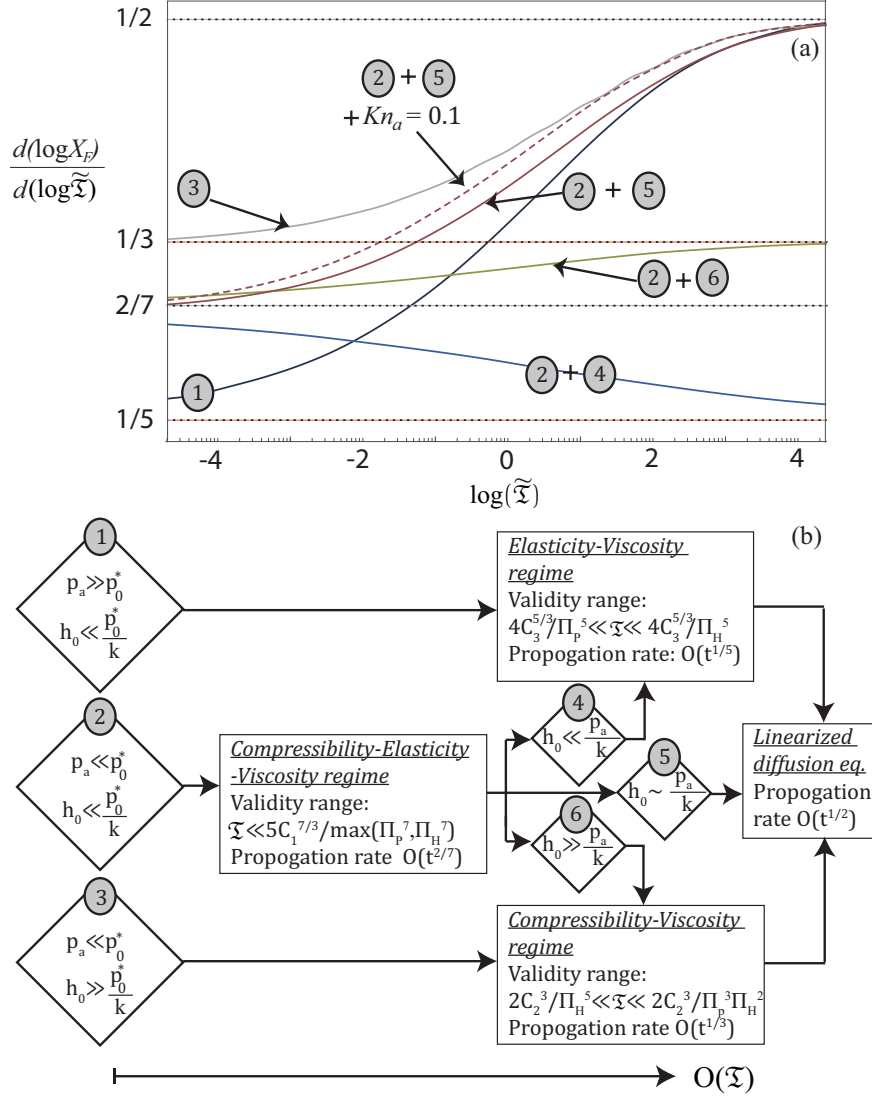


Figure 3: Propagation regimes of gaseous viscous peeling in a 2D gap bounded by linearly elastic substrates for different time-scales and physical parameters. (a) Numerical computation of the propagation front velocity (logarithmic derivative) from (2.5) vs. the theoretical limits given by (3.3)-(3.5). Line (1) corresponds to $(M, \Pi_H, \Pi_P) = (3.8 \times 10^{-3}, 2 \times 10^{-3}, 2)$; line (2) + (4) corresponds to $(M, \Pi_H, \Pi_P) = (2.86 \times 10^{-4}, 0, 1 \times 10^{-2})$; line (2) + (5) corresponds to $(M, \Pi_H, \Pi_P) = (2.95 \times 10^{-4}, 5 \times 10^{-3}, 1 \times 10^{-2})$; line (2) + (6) corresponds to $(M, \Pi_H, \Pi_P) = (2.77 \times 10^{-4}, 5 \times 10^{-3}, 0)$; line (3) corresponds to $(M, \Pi_H, \Pi_P) = (5.35 \times 10^{-4}, 0.15, 10^{-4})$. Time is rescaled according to the average time presented in the figure, $\tilde{T} = 10^7 \tau$. (b) A flow-chart diagram describing the different dominant balances, transitions between regimes and propagation time-scales as a function of initial gauge pressure p_0^* , background pressure p_a , channel stiffness k and prewetting layer thickness h_0 .

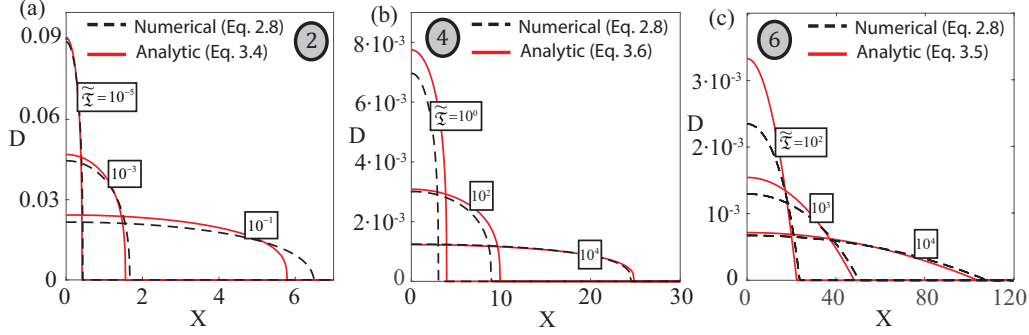


Figure 4: Convergence of the numerical deformation profiles to the theoretical results (3.3), (3.4) and (3.5) corresponding to the respective values of (M, Π_H, Π_P) presented in figure 3. Panels (a), (b) and (c) present convergence along lines (2)+(6) (stage (2)), (2)+(4) (stage (4)) and (2)+(6) (stage (6)), respectively.

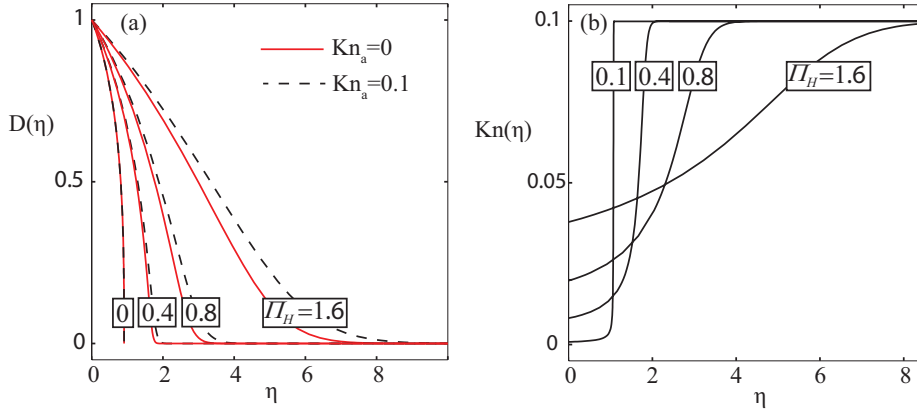


Figure 5: Self-similar solutions with weak-rarefaction effects for $\Pi_P = \Pi_H$ and $\sigma = 1$. (a) Self-similar deformation profile as a function of the prewetting thickness ratio Π_H for $Kn_a = 0$ (smooth lines) and $Kn_a = 0.1$ (dashed lines). (b) Local Knudsen as a function of η for various values of Π_H for $Kn_a = 0.1$. Solution based on numerical integration of (3.6).

where $(N, C) = (5, \Pi_P)$ for the limit of $\Pi_P, \Pi_H \ll D$ (viscous-elastic-compressibility regime) or the symmetric case of $\Pi_P = \Pi_H$; $(N, C) = (2, \Pi_P)$ for the limit of $\Pi_H \gg \Pi_P, D$ (viscous-compressibility regime); $(N, C) = (4, \Pi_H)$ for the limit of $\Pi_P \gg \Pi_H, D$ (viscous-elastic regime) and finally, $(N, C) = (1, 0)$ for the linear limit of $\Pi_P, \Pi_H \gg D$ (viscous regime) .

REFERENCES

- ARKILIC, E. B., BREUER, K. S. & SCHMIDT, M. A. 2001 Mass flow and tangential momentum accommodation in silicon micromachined channels. *J. Fluid Mech.* **437**, 29–43.
- ARKILIC, E. B., SCHMIDT, M. A. & BREUER, K. S. 1997 Gaseous slip flow in long microchannels. *J. Microelectromech. Syst.* **6**, 167–178.
- AUBERT, C. & COLIN, S. 2001 High-order boundary conditions for gaseous flows in rectangular microchannels. *Microscale Therm. Eng.* **5**, 41–54.

- BARENBLATT, G. I. 1952 On some unsteady fluid and gas motions in a porous medium. *Prikl. Mat. Mekh.* **16**(1), 67–78 (in Russian).
- CERCIGNANI, C. 2000 *Rarefied Gas Dynamics*. Macmillan and co.
- CHAPMAN, S. & COWLING, T. G. 1952 *The Mathematical Theory of Non-uniform Gases: An Account of the Kinetic Theory of Viscosity, Thermal Conduction and Diffusion of Gases, Notes Added in 1951*. Cambridge University Press.
- ELBAZ, S. B. & GAT, A. D. 2016 Axial creeping flow in the gap between a rigid cylinder and a concentric elastic tube. *Journal of Fluid Mechanics* **806**, 580–602.
- GAD-EL-HAK, M. 1999 The fluid mechanics of microdevices. *J. Fluid Engng.* **121**, 5–33.
- GAT, A. D., FRANKEL, I. & WEIHS, D. 2008 Gas flows through constricted shallow micro-channels. *Journal of Fluid Mechanics* **602**, 427–442.
- GAT, A. D., FRANKEL, I. & WEIHS, D. 2009 A higher-order hele-shaw approximation with application to gas flows through shallow micro-channels. *Journal of Fluid Mechanics* **638**, 141–160.
- GAT, A. D., FRANKEL, I. & WEIHS, D. 2010a Compressible flows through micro-channels with sharp edged turns and bifurcations. *Microfluidics and Nanofluidics* **8** (5), 619–629.
- GAT, A. D., FRANKEL, I. & WEIHS, D. 2010b Gas flows through shallow t-junctions and parallel microchannel networks. *Physics of Fluids* **22** (9), 092001.
- GAVER, D. P., HALPERN, D., JENSEN, O. E. & GROTHBERG, J. B. 1996 The steady motion of a semi-infinite bubble through a flexible-walled channel. *Journal of Fluid Mechanics* **319**, 25–65.
- HEWITT, I. J., BALMFORTH, N. J. & DE BRUYN, J. R. 2015 Elastic-plated gravity currents. *European Journal of Applied Mathematics* **26** (01), 1–31.
- HO, C. M. & TAI, Y. C. 1998 Micro-electro-mechanical-systems (mems) and fluid flows. *Annu. Rev. Fluid Mech.* **30**, 579–612.
- HODGES, S. R. & JENSEN, O. E. 2002 Spreading and peeling dynamics in a model of cell adhesion. *Journal of Fluid Mechanics* **460**, 381–409.
- HOSOI, A. E. & MAHADEVAN, L. 2004 Peeling, healing, and bursting in a lubricated elastic sheet. *Physical review letters* **93** (13), 137802.
- HUPPERT, H. E. 1982 The propagation of two-dimensional and axisymmetric viscous gravity currents over a rigid horizontal surface. *Journal of Fluid Mechanics* **121**, 43–58.
- JANG, J. & WERELEY, S. 2004 Pressure distributions of gaseous slip flow in straight and uniform rectangular microchannels. *Microfluid Nanofluid* **1**, 41–51.
- LEE, W. Y., WONG, M. & ZOHAR, Y. 2001 Gas flow in microchannels with bends. *J. Micromesh. Microeng.* **11**, 635–644.
- LEE, W. Y., WONG, M. & ZOHAR, Y. 2002 Pressure loss in constriction microchannels. *J. Microelectromech. Syst.* **11**, 236–244.
- LISTER, J. R., PENG, G. G. & NEUFELD, J. A. 2013 Viscous control of peeling an elastic sheet by bending and pulling. *Physical review letters* **111** (15), 154501.
- LIU, J., TAI, Y.-C. & HO, C.-M. 1995 MemS for pressure distribution studies of gaseous flows in microchannels. In *proceedings of the IEEE micro electro mechanical systems*, pp. 209–215.
- MCEWAN, A. D. & TAYLOR, G. I. 1966 The peeling of a flexible strip attached by a viscous adhesive. *Journal of Fluid Mechanics* **26** (01), 1–15.
- ORON, A., DAVIS, S. H. & BANKOFF, S. G. 1997 Long-scale evolution of thin liquid films. *Reviews of modern physics* **69** (3), 931.
- PONG, K.-C., HO, C.-M., LIU, J. & TAI, Y.-C. 1994 Non-linear pressure distribution in uniform microchannels. *ASME-PUBLICATIONS-FED* **197**, 51–51.
- TAYLOR, G.I. & SAFFMAN, P.G. 1957 Effects of compressibility at low reynolds number. *J. Phys. Chem. Ref. Data* **24**, 553–562.
- THOREY, C. & MICHAUT, C. 2016 Elastic-plated gravity currents with a temperature-dependent viscosity. *Journal of Fluid Mechanics* **805**, 88–117.
- YOUNG, Y-N & STONE, HA 2017 Long-wave dynamics of an elastic sheet lubricated by a thin liquid film on a wetting substrate. *Physical Review Fluids* **2** (6), 064001.
- YU, Z.T.F., LEE, Y.-K., WONG, M. & ZOHAR, Y. 2005 Fluid flows in microchannels with cavities. *J. Microelectromech. Syst.* **14**, 1386–1398.
- ZOHAR, Y., LEE, S. Y. K., LEE, W. Y., JIANG, L. & TONG, P. 2002 Subsonic gas flow in a straight and uniform microchannel. *J. Fluid Mech.* **472**, 125–151.